First-principles calculations of properties of orthorhombic iron carbide Fe_7C_3 at the Earth's core conditions

Zamaan Raza,[1] Nina Shulumba,[1,2] Nuala M. Caffrey,[1] Leonid Dubrovinsky,[3] and Igor A. Abrikosov[1,4,5]

[1]*Department of Physics, Chemistry and Biology (IFM), Linköping University, SE-581 83, Linköping, Sweden*

[2]*Functional Materials, Saarland University, Campus D3 3, D-66123 Saarbrücken, Germany.*

[3]*Bayerisches Geoinstitut, Universität Bayreuth, 95440 Bayreuth, Germany*

[4]*Materials Modeling and Development Laboratory, NUST "MISIS," 119049 Moscow, Russia*

[5]*LACOMAS Laboratory, Tomsk State University, 634050, Tomsk, Russia*

(Received 6 March 2015; revised manuscript received 1 June 2015; published 24 June 2015)

A recently discovered phase of orthorhombic iron carbide o-Fe_7C_3 [Prescher *et al.*, Nat. Geosci. **8**, 220 (2015)] is assessed as a potentially important phase for interpretation of the properties of the Earth's core. In this paper, we carry out first-principles calculations on o-Fe_7C_3, finding properties to be in broad agreement with recent experiments, including a high Poisson's ratio (0.38). Our enthalpy calculations suggest that o-Fe_7C_3 is more stable than Eckstrom-Adcock hexagonal iron carbide (h-Fe_7C_3) below approximately 100 GPa. However, at 150 GPa, the two phases are essentially degenerate in terms of Gibbs free energy, and further increasing the pressure towards Earth's core conditions stabilizes h-Fe_7C_3 with respect to the orthorhombic phase. Increasing the temperature tends to stabilize the hexagonal phase at 360 GPa, but this trend may change beyond the limit of the quasiharmonic approximation.

DOI: 10.1103/PhysRevB.91.214112 PACS number(s): 61.66.−f, 62.20.−x, 91.60.Ed

I. INTRODUCTION

The core of the Earth is believed to be predominantly comprised of iron, the only heavy element with a sufficiently high cosmic abundance to account for its overall mass and density. However, iron cannot be the sole constituent because the density of such a core would be up to 10% higher than is observed [1,2]. Furthermore, sound velocities in pure iron extrapolated to Earth's core conditions are inconsistent with seismological observations [3].

Taking into account cosmochemical considerations such as abundance and solubility in iron under the conditions of the Earth's formation, the most likely candidates for alloying elements are H, C, O, Si, and S [4]. The identification of the actual species (singular or plural), and the exact nature of their incorporation in the core, has been the subject of considerable debate.

There is evidence to suggest that there may be a significant amount of carbon in the Earth's core [5]. Cementite iron carbide (Fe_3C) was initially proposed as the most likely carbon vehicle [6]. However, consideration of the pressure-induced transition of Fe_3C from a ferromagnetic to a nonferromagnetic state, as evidenced by *ab initio* calculations [7], sound velocity measurements [8], and high pressure experiments [9], results in conflicting evidence.

More recent calculations, based on better knowledge of the magnetic transition behavior of iron carbides with temperature and pressure, suggest that the Eckstrom-Adcock hexagonal phase of Fe_7C_3 [10] (henceforth referred to as h-Fe_7C_3) is a more convincing candidate in some respects. It is more stable than Fe_3C at core conditions and is expected to be the first crystallizing phase at pressures up to 360 GPa [11,12]. Like cementite Fe_3C, it is magnetic at low pressure and undergoes a magnetic collapse (high spin to low spin, accompanied by a decrease in the rate of change of the bulk modulus) at high pressure, at 67 GPa and 0 K according to *ab initio* calculations [13] and 53 GPa according to experiment [14]. At pressures above this spin transition, the sound velocity increases with pressure at a much lower rate, which may explain the anomalously low sound velocity in the Earth's core without the need to invoke partial melting or high-temperature effects [15].

Hexagonal Fe_7C_3 is not the only possibility. Theoretical structure prediction calculations at core pressures and zero kelvin [16,17] have uncovered new Fe_3C phases that are more stable than cementite at core pressures, and a stoichiometry which has not been previously discussed in relation to the Earth's core, Fe_2C. These studies suggest that Fe_7C_3 decomposes to Fe_3C and Fe_2C at core pressures, but there is a lack of experimental evidence to support their claims. Although experiments have ruled out the coexistence of pure iron and carbon at high pressures and temperature [18], *ab initio* calculations suggest that significant amounts (up to 6 at.%) of carbon can exist in crystalline phases of iron as interstitial defects under high pressure, suggesting the existence of an iron-carbon alloy [19].

A new orthorhombic phase of Fe_7C_3 (referred to as o-Fe_7C_3) has very recently been discovered [20]. High pressure diamond anvil cell experiments suggest that o-Fe_7C_3 is the crystallizing phase at the conditions of the Earth's outer core, rather than h-Fe_7C_3. Moreover, extrapolations to higher pressures and temperatures suggest that it accounts for the anomalously high Poisson ratio and low shear wave velocity of the core. The properties of o-Fe_7C_3 were only measured up to 180 GPa, but it is known that the relative stabilities of the phases can change dramatically as a function of temperature and pressure. First-principles calculations offer a route to directly probe the iron carbide phase diagram at the conditions of the Earth's core. In this paper, we use density functional theory (DFT) calculations to compare the stability of o-Fe_7C_3 with the well characterized h-Fe_7C_3 at both experimental pressures and the pressure of the Earth's inner core, and discuss its potential geophysical importance. If it is present in the

Earth's core, Fe_7C_3 would have a tremendous impact on the Earth's carbon budget, and by extension geophysical models of the Earth's formation; in this case, the core would comprise the largest carbon reservoir on the planet.

II. COMPUTATIONAL METHODOLOGY

All *ab initio* calculations were performed with the VASP DFT code [21], at the generalized gradient approximation (GGA) level, using the Perdew-Burke-Ernzerhof (PBE) exchange-correlation functional [22]. Core electrons were approximated using projector augmented-wave (PAW) pseudopotentials [23,24], and valence electrons were represented with a plane wave basis set with a cutoff energy of 600 eV. The $3d$ and $4s$ electrons of Fe (8 total) and the $2s$ and $2p$ electrons of C (4 total) were treated explicitly as valence. The Brillouin zone was sampled using a Monkhorst-Pack grid of k points [25] dependent on the phase: $6 \times 6 \times 6$ for h-Fe_7C_3 and $2 \times 6 \times 2$ for o-Fe_7C_3, with a denser $3 \times 9 \times 3$ grid for electronic structure calculations. In order to ensure accurate force constants for phonon calculations, electronic energies were converged to a threshold of 1×10^{-8} eV between ionic steps and forces to a tolerance of 1×10^{-8} eV Å^{-1}. Spin polarized calculations were also performed to determine the relative stability of magnetic and nonmagnetic phases.

Phonon dispersions and free energy calculations were performed using the PHONOPY package [26]. Real-space force constants were calculated using supercell method and density functional perturbation theory (DFPT) as implemented in VASP, with a $2 \times 2 \times 2$ supercell for h-Fe_7C_3 and a $1 \times 3 \times 1$ supercell for o-Fe_7C_3. The Brillouin zone was sampled using a $2 \times 2 \times 4$ k-point mesh for the h-Fe_7C_3 supercell and only the gamma point for o-Fe_7C_3, since it was found that a $2 \times 2 \times 2$ mesh had an insignificant effect on free energies. Helmholtz free energies were computed for both structures at five volumes starting from 150 GPa and 360 GPa, then corrected for thermal expansion using the quasiharmonic approximation, resulting in Gibbs free energies in both pressure regimes.

III. RESULTS AND DISCUSSION

A. Crystal structure and magnetism

The o-Fe_7C_3 structure has space group $Pbca$ and a unit cell containing 80 atoms consisting of CFe_6 trigonal prisms (Fig. 1) [20]. The PBE-optimized structure at zero pressure has lattice parameters $a = 10.80$, $b = 3.95$, and $c = 12.50$, corresponding to a volume of 533.7 Å^3. The c/a and b/a ratios agree with the experimental values to within 0.3%.

Figure 2(a) shows the total volume and energy of the spin polarized and nonspin polarized calculations as a function of pressure. PBE calculations underestimate the volume by 2.3% relative to experiments at low pressures (0–10 GPa), decreasing to 1% at high pressures (100–150 GPa), i.e. a good agreement. Reoptimizing the structure using a spin polarized solution increases the cell volume by 4.3% relative to the structure relaxed with an unpolarized solution at 0 GPa. At this point the ferromagnetic state is 130 meV/Fe atom lower in energy that the nonmagnetic solution. The ferromagnetic state becomes progressively less energetically favorable with increasing pressure until a magnetic to nonmagnetic transition occurs at 120 GPa as calculated with PBE. This transition is preceded by another at approximately 40 GPa, evident from a change of slope in the volume difference curve [Fig. 2(b)]. This transition can also be seen by a large drop in the moment associated with two of the Fe sites, shown in Fig. 3(a). o-Fe_7C_3 has seven symmetry-distinct sites for the Fe atoms, with PBE-calculated magnetic moments on these sites ranging

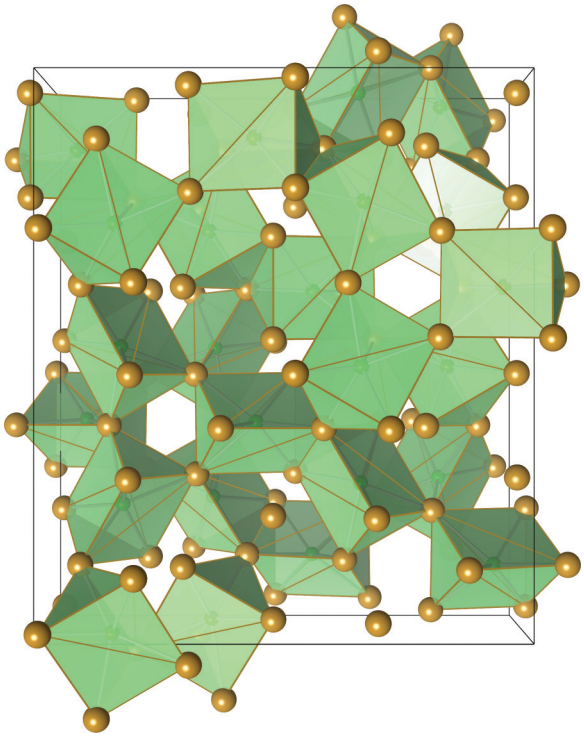

FIG. 1. (Color online) The unit cell of the o-Fe_7C_3 phase (space group $Pbca$). Fe atoms are brown and C atoms are green. CFe_6 trigonal prism polyhedra are shown.

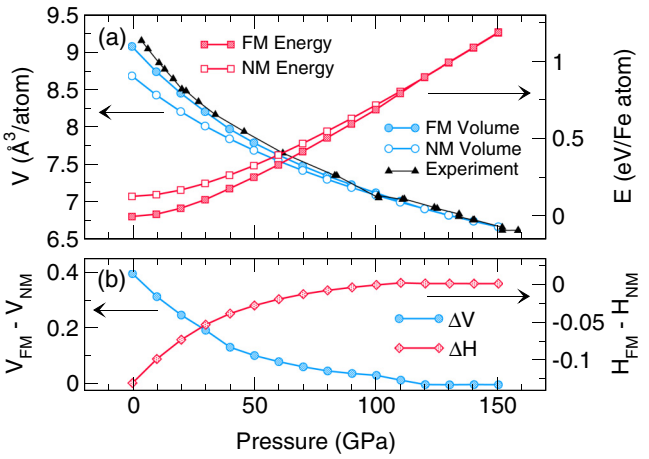

FIG. 2. (Color online) (a) Volume (blue lines) and total energy (red lines) of the spin polarized (filled symbols) and nonspin polarized (open symbols) phases for o-Fe_7C_3. (b) The enthalpy difference between the spin polarized and nonspin polarized phases, given per Fe atom. The black triangles are the experimentally measured volumes taken from Ref. [20].

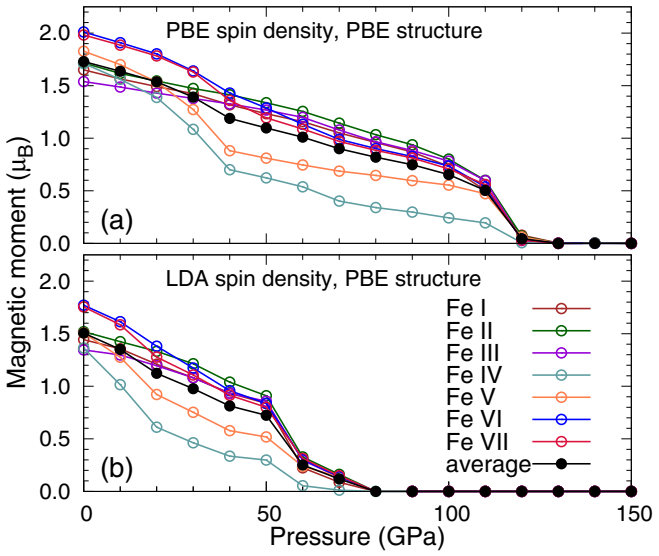

FIG. 3. (Color online) Calculated magnetic moment per atom for each Fe type (colored lines with symbols) and for the total average magnetic moment (black line). The upper panel displays the magnetic moments calculated with the PBE-relaxed structure and the PBE spin density. The lower panel uses the same PBE-relaxed structures, with magnetic moments calculated from the LDA spin density.

between 1.5 and 2 μ_B, and an average value of 1.7 μ_B at zero pressure. The response of these moments to pressure depends on how their local environment changes. Two sites in particular initially experience a rapid drop in magnetic moment up to 40 GPa after which they become relatively stable.

The total density of states is shown in Fig. 4 for o-Fe_7C_3 experiencing pressures of 0, 70, 150, and 360 GPa. Energies around the Fermi level are dominated by states with Fe d character, with the C states predominantly found at energies 4 eV below the Fermi level. The material remains metallic at all pressures considered. At 0 GPa an exchange splitting leads to a large energy shift between the majority and minority d states. Almost the entire moment is located on the Fe atoms, with a small induced moment (0.1 μ_B) on the C atoms aligned antiferromagnetically to that on the Fe atoms. With increasing pressure, the bandwidths increase while the size of the band gaps present in the valence band decrease. The Fe atoms labeled Fe IV and Fe V (c.f. Fig. 3) are different, and experience a sharper drop in magnetic moment with pressure than the other Fe atoms. Both have a large peak in the d_{yz} minority states just above the Fermi level at zero pressure which is shifted lower in energy with increasing pressure, becoming fully occupied. Conversely, for the others, this state is occupied even at zero pressure. This can be seen by comparing Figs. 4(a) and 4(b) which show the DOS calculated at 70 GPa for one of the two different sites, Fe-IV, and one of the typical sites, Fe-I (i.e., experiencing a much slower reduction in moment with pressure). Similarly, the majority states of Fe-IV and Fe-V become significantly broader than in the others with increasing pressure. The result is a smaller magnetic moment localized on these two Fe sites.

We conclude this section with a comparison between the transition pressures found theoretically and experimentally. Mössbauer spectroscopy indicates a ferromagnetic to paramagnetic transition at 16 GPa and a paramagnetic to nonmagnetic transition at 70 GPa [20]. Although pressure of the transition to a nonmagnetic state is considerably overestimated here, conflicts between theoretical and experimental magnetic transition pressures are a common problem for iron carbides, in particular for cementite Fe_3C [7,27]. While PBE is known to overestimate magnetic moments [28], LDA consistently underestimates the cell volumes (by 3% relative to PBE in the case of o-Fe_7C_3, at 150 GPa). Such drastic structural changes have a knock-on effect on the electronic structure, to the point that it is impossible to rely on the magnetic moments of LDA-optimized structures. Calculating the LDA charge density of a PBE-optimized structure results in a cancellation

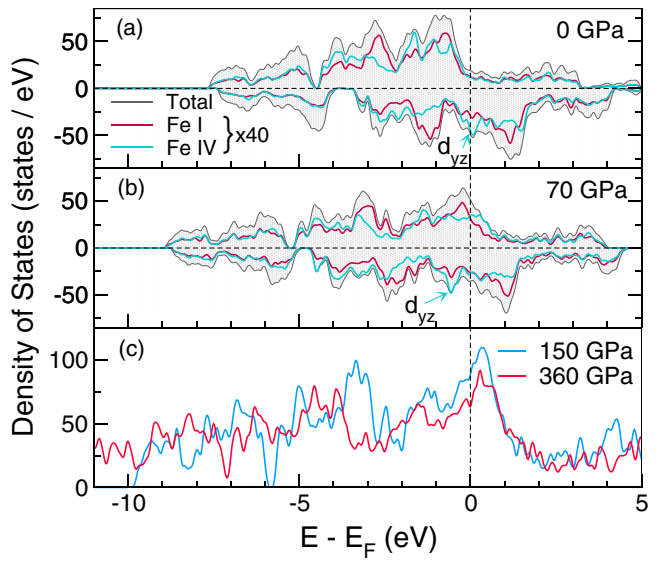

FIG. 4. (Color online) The total electronic density of states for o-Fe_7C_3 calculated at (a) 0 GPa, (b) 70 GPa, and (c) 150 GPa and 360 GPa. The spin-resolved DOS projected onto Fe I and Fe IV are also shown at 0 and 70 GPa (note multiplying factor of 40 in scale for projected density of states). The dashed line at 0 eV denotes the Fermi level. The structures were relaxed using PBE and the spin density calculated using PBE.

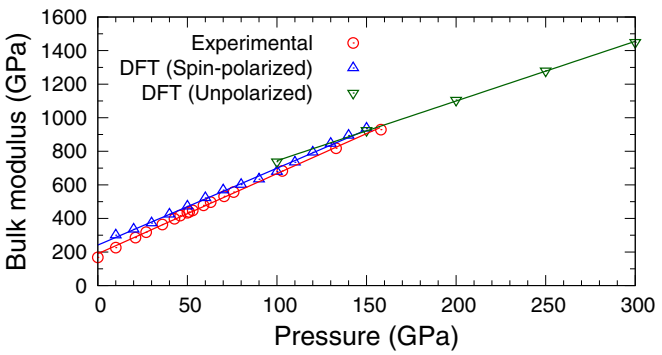

FIG. 5. (Color online) Bulk modulus (K) of o-Fe_7C_3 as a function of pressure. Experimental data taken from Ref. [20] are compared with DFT spin polarized and unpolarized results. After the PBE ferromagnetic to nonmagnetic transition (120 GPa), the bulk modulus changes at a lower rate with increasing pressure, indicating that separate equations of state are required for the magnetic and nonmagnetic configurations.

TABLE I. The density (ρ,kg m^{-3}), bulk modulus (K), shear modulus (G), and 9 derived symmetry-unique elastic constants (in GPa) of o-Fe_7C_3 at 150 and 360 GPa.

P (GPa)	ρ	K	G	c_{11}	c_{22}	c_{33}	c_{12}	c_{23}	c_{31}	c_{44}	c_{55}	c_{66}
150	10625	7432	2030	1073	931	1116	600	599	585	135	169	266
360	12579	12749	3294	1796	1572	1864	1080	1040	1000	251	275	417

of errors that reduces the magnetic moments [29] and therefore the magnetic-nonmagnetic transition pressure. This can be seen in Fig. 3(b) which shows the magnetic moments as a function of pressure as calculated with the LDA-calculated spin density at the PBE relaxed structure. The magnetic moment now vanishes at 80 GPa, which is consistent with the experimental magnetic-to-nonmagnetic transition of 70 GPa.

B. Mechanical properties

In Fig. 5, we plot the calculated bulk modulus of o-Fe_7C_3 as a function of pressure, together with experimental results [20]. Spin polarized calculations were employed up to 150 GPa, after which there is a transition to a nonmagnetic state. This is manifested as a decrease in the rate of stiffening as the pressure increases, and demonstrates that, as for cementite Fe_3C and h-Fe_7C_3, it is not valid to extrapolate the ferromagnetic equation of state to Earths core conditions; instead, another equation of state is required.

By calculating the elastic constants (Table I), we were able to compute the mono-crystalline bulk and shear moduli, and subsequently zero Kelvin Poisson's ratio ν using the expression

$$\nu = \frac{3K - 2G}{2(3K + G)},$$

where K is the bulk modulus and G is the shear modulus. These values were found to be in good agreement with experiment [20] at 150 GPa, including a calculated ν of 0.375 compared with the measured value of 0.39. At the pressure of the Earth's core, 360 GPa, Poisson's ratio was found to be very similar, with a value of 0.381. This supports the claim that carbon alloying may be responsible for the anomalously high Poisson's ratio of the Earth's core, 0.44 [3], particularly since the Poisson ratio is expected to increase with temperature.

The monocrystalline longitudinal (compressional) and both components of the transverse (shear) sound velocity were calculated by solving the Christoffel equation using the computed (zero temperature) elastic constants. There is considerable anisotropy in the orthorhombic cell, manifested most obviously in the *b* lattice parameter, which changes at a different rate to the others as a function of pressure. Sound velocities are therefore plotted as a function of angle about the origin for the 001, 100, and 010 planes in Fig. 6. The experimental velocities at 158 GPa and 300 K are 10.7 km s^{-1} for v_P and 4.6 km s^{-1} for v_S [20], a reasonable agreement with our calculations considering the pressure and temperature difference, and that any real sample will not be a single crystal. (See Table II).

C. Enthalpy

h-Fe_7C_3 is 4.6 meV higher in enthalpy than o-Fe_7C_3 at 150 GPa in the local density approximation (LDA). This difference is essentially the same (3.4 meV) using the PBE GGA functional. Together with good agreement of structural parameters with experiment, we can treat our choice of functional in this regard with confidence.

The enthalpy difference between h-Fe_7C_3 and o-Fe_7C_3 is shown in Fig. 7. It initially seems that the o-Fe_7C_3 phase is more stable at pressures below approximately 100 GPa. There are some caveats to this observation: First, the enthalpy difference is extremely small, around 2 meV/atom at 150 GPa, which is smaller than the typical error in a DFT calculation (around 5 meV per atom). Since the calculated energy difference is so small, it is likely that the zero Kelvin transition

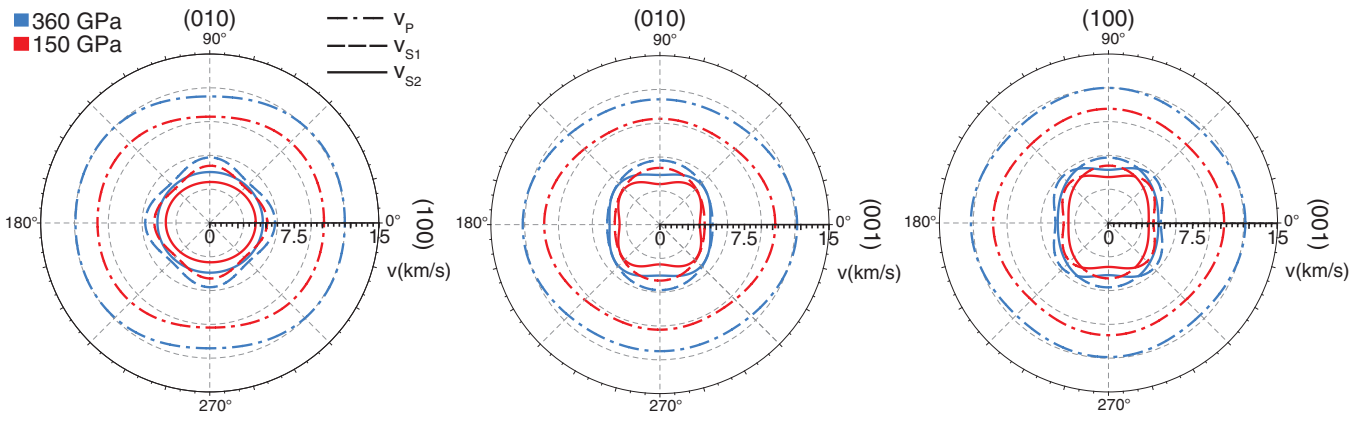

(a) 001 (b) 100 (c) 010

FIG. 6. (Color online) Longitudinal sound velocity (v_p) and components of transverse sound velocity (v_{s1}, v_{s2}) in km s^{-1} in the 001, 100, and 010 directions for o-Fe_7C_3.

TABLE II. Sound velocity ranges (km s^{-1}) and anisotropies A (%) of o-Fe_7C_3.

P (GPa)	v_P	v_{S1}	v_{S2}	A_{vP}	A_{vS1}	A_{vS2}
150	9.3–10.1	4.3–5.0	3.6–4.7	8.8	16.1	31.3
360	11.2–12.0	4.9–5.8	4.5–5.5	7.9	18.0	22.5

pressure is underestimated, considering experiments suggest that o-Fe_7C_3 is more stable than h-Fe_7C_3 at 150 GPa [20]. Second, both phases are magnetic at the low end of the pressure scale, and it has been shown that changes in the magnetic state in different iron carbides are associated with changes in the physical properties [13,14,27]. The calculated enthalpies suggest o-Fe_7C_3 is the more stable phase by a significant margin in the magnetic regime. We note, however, that these values are calculated assuming a ferromagnetic state whereas a paramagnetic regime has been observed experimentally [20]. Thirdly, the enthalpy only describes the stability of the phases at absolute zero, yet we are interested in the stability at the conditions of the Earth's core. Further calculations are therefore necessary to assess the relative stability of the two phases.

D. Free energy and the effect of temperature

Owing to the high computational expense of phonon calculations, we focus on two pressures: the high end of the experimental regime, 150 GPa, and the estimated pressure of the Earth's inner core, 360 GPa. The phonon density of states (Fig. 8) shows no negative frequencies, therefore o-Fe_7C_3 is dynamically stable at both pressures, within the limits of the harmonic approximation.

As the temperature of the Earth's core is estimated to be between 5000 and 7000 K we also need to include the contribution of vibrational entropy, and thus compare the Gibbs free energies of the two phases. Calculating free energies from the phonon density of states in the harmonic approximation is a first step to understanding the effect of high temperatures on these phases.

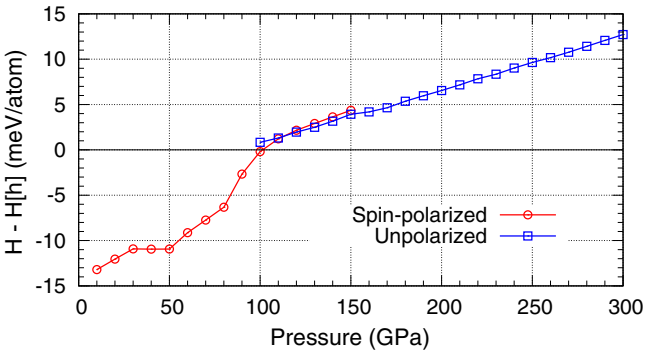

FIG. 7. (Color online) Enthalpy difference of o-Fe_7C_3 with respect to h-Fe_7C_3. The enthalpy differences for spin-polarized and unpolarized DFT calculations are plotted separately. It should be noted that the magnetic to nonmagnetic transition occurs at different pressures for h- and o-Fe_7C_3, hence the lack of a smooth curve below 100 GPa.

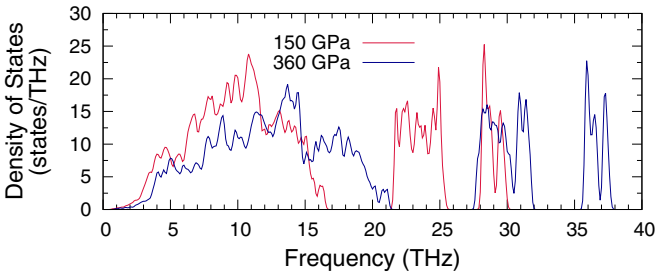

FIG. 8. (Color online) Phonon density of states of o-Fe_7C_3 at 150 GPa and 360 GPa.

Starting from fixed volume calculations of the Helmholtz free energy at 150 GPa and 360 GPa, at a temperature of 0 K, we take into account the effect of thermal expansion in the quasiharmonic approximation to obtain the Gibbs free energies of the two phases as a function of temperature. This is shown in Fig. 9.

We first note that at 150 GPa and 0 K, the free energy of o-Fe_7C_3 is 6 meV/atom higher than that of h-Fe_7C_3. This should be compared to a difference of 3.4 meV when vibrational effects are excluded showing that the zero point energy increases the stability of o-Fe_7C_3 by approximately 2.6 meV compared to h-Fe_7C_3. This gap decreases to 2 meV/atom at 1000 K. The energy difference is small over the whole temperature range, but the trend is towards the stabilization of o-Fe_7C_3 with respect to h-Fe_7C_3 as the temperature increases. Assuming this behavior continues into the anharmonic regime at extreme temperatures (which is by no means guaranteed), this tends to agree with experiments in which o-Fe_7C_3 was crystallized from a melt at 180 GPa and 3500 K. At 360 GPa, however, there is a significant free energy difference between the two phases, h-Fe_7C_3 being more stable by in excess of 50 meV/atom over the temperature range. This trend continues with increasing temperature—again with the caveat that we have not considered anharmonic effects at higher

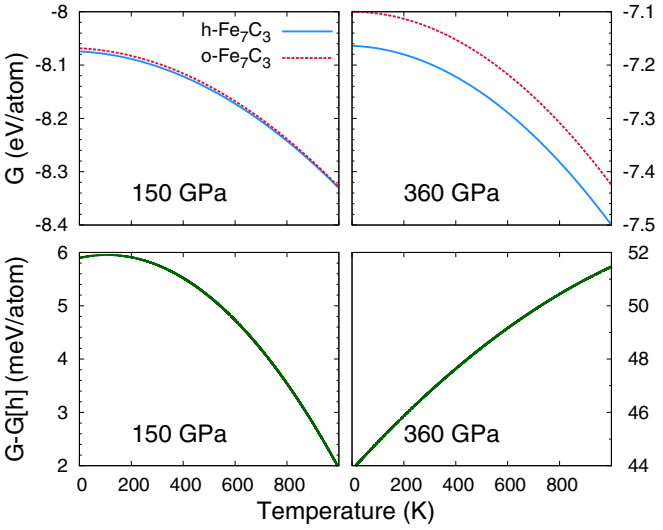

FIG. 9. (Color online) Upper panels: Gibbs free energies of the h-Fe_7C_3 and o-Fe_7C_3 structures at 150 GPa and 360 GPa. Lower panels: Gibbs free energy difference between the two phases.

temperatures—so we conclude that the new orthorhombic phase would not be competitive at the temperature and pressure conditions of the Earth's core according to DFT calculations.

IV. CONCLUSIONS

First-principles calculations were used to assess the stability of two candidates for iron carbide phases at the Earth's core: hexagonal Eckstrom-Adcock Fe_7C_3, and a recently discovered orthorhombic Fe_7C_3 phase [20]. Spin-polarized DFT calculations demonstrate that there is a magnetic to nonmagnetic transition as the pressure increases over 120 GPa; this is associated with a decrease in the rate of stiffening, i.e., the bulk modulus increases at a lower rate as the pressure increases. Static DFT calculations suggest that o-Fe_7C_3 is more stable below a pressure of 100 GPa, although the enthalpy differences between the two are very small over a large pressure range, up to approximately 200 GPa. Taking the effects of temperature into account, vibrational entropy stabilizes o-Fe_7C_3 with respect to the hexagonal phase at 150 GPa, and by extrapolation, becomes more stable in excess of 1000 K. However, at the pressure of the Earth's core (360 GPa), o-Fe_7C_3 is no longer competitive in our theoretical calculations. The possibility remains that Fe_7C_3 may decompose to more stable stoichiometries such as Fe_2C and Fe_3C, as suggested by *zero temperature* structure prediction calculations [17]. However, confirmation would require many more expensive free energy calculations which are beyond the scope of this paper.

We emphasize that the thermodynamic calculations were carried out in the quasiharmonic approximation. Although this is valid at intermediate temperatures, perhaps up to around two thirds of the melting temperature depending on the nature of the system, it is impossible to draw a strong conclusion on the relative stability of these phases at the temperatures of the inner core (5000–7000 K), which appears to be approximately the melting temperature of Fe_7C_3 [12,30]. Our calculations are largely in good agreement with the available experimental data but do not include strong correlation effects via, for example, the DFT+U method. One would not expect correlation effects to make a significant difference at such high pressures for our purposes, but there are exceptions to this trend [31], and it would be instructive to consider them in future studies.

The carbon budget of the Earth is poorly constrained and has been estimated as between 0.2 wt.% and 4 wt.% [12]. Moreover, there is uncertainty in the distribution of carbon between the metallic core and silicate mantle, due to poor constraints on carbon solubility in metals and partitioning behavior; however the maximum carbon content of the core is estimated to be 6–7 wt.% [32]. Fe_7C_3 is approximately 9 wt.% carbon, which is significantly too high to make it a credible candidate for the dominant phase in the core, although it may be a competing phase. Nonstoichiometric iron carbides such as solid solutions or substitutional carbon defects in hcp iron could account for this discrepancy but present a considerable challenge to model. Further study is therefore required, including full anharmonic treatments of these phases to assess their stabilities at high temperatures.

ACKNOWLEDGMENTS

The authors wish to acknowledge the Swedish Foundation for Strategic Research (SSF) program FUNCASE as the main sponsor, and support from the Swedish Research Council (VR) Grant No. 621-2011-4426, support from SSF programs "Multifilms" and SRL Grant No. 10-0026. N.S. acknowledges the financial support from the Erasmus Mundus Joint European Doctoral Programme DocMASE. All calculations were performed using the supercomputer resources of the Swedish National Infrastructure for Computing (SNIC) National Supercomputing Center (NSC). I.A.A. acknowledges the support from the Grant of Ministry of Education and Science of the Russian Federation (Grant No. 14.Y26.31.0005) and Tomsk State University Academic D. I. Mendeleev Fund Program (Project No. 8.1.18.2015).

[1] F. Birch, J. Geophys. Res. **57**, 227 (1952).
[2] F. Birch, J. Geophys. Res. **69**, 4377 (1964).
[3] A. M. Dziewonski and D. L. Anderson, Phys. Earth Planet. In. **25**, 297 (1981).
[4] J.-P. Poirier, Phys. Earth Planet. In. **85**, 319 (1994).
[5] B. J. Wood, J. Li, and A. Shahar, Rev. Mineral. Geochem. **75**, 231 (2013).
[6] B. J. Wood, Earth Planet. Sci. Lett. **117**, 593 (1993).
[7] L. Vočadlo, J. Brodholt, D. B. Dobson, K. S. Knight, W. G. Marshal, G. D. Price, and I. G. Wood, Earth Planet. Sci. Lett. **203**, 567 (2002).
[8] L. Gao, B. Chen, J. Wang, E. E. Alp, J. Zhao, M. Lerche, W. Sturhahn, H. P. Scott, F. Huang, Y. Ding, S. V. Sinogeikin, C. C. Lundstrom, J. D. Bass, and J. Li, Geophys. Res. Lett. **35**, L17306 (2008).
[9] S. Ono and K. Mibe, Phys. Earth Planet. In. **180**, 1 (2010).
[10] H. C. Eckstrom and W. A. Adcock, J. Am. Chem. Soc. **72**, 1042 (1950).
[11] Y. Nakajima, E. Takahashi, T. Suzuki, and K. Funakoshi, Phys. Earth Planet. In. **174**, 202 (2009).
[12] O. T. Lord, M. J. Walter, R. Dasgupta, D. Walker, and S. M. Clark, Earth Planet. Sci. Lett. **284**, 157 (2009).
[13] M. Mookherjee, Y. Nakajima, G. Steinle-Neumann, K. Glazyrin, X. Wu, L. Dubrovinsky, C. McCammon, and A. Chumakov, J. Geophys. Res. **116**, B04201 (2011).
[14] B. Chen, L. Gao, B. Lavina, P. Dera, E. E. Alp, J. Zhao, and J. Li, Geophys. Res. Lett. **39**, L18301 (2012).
[15] B. Chen, Z. Li, D. Zhang, J. Liu, M. Y. Hu, J. Zhao, W. Bi, E. E. Alp, Y. Xiao, P. Chow, and J. Li, Proc. Natl. Acad. Sci. USA **111**, 17755 (2014).
[16] G. L. Weerasinghe, R. J. Needs, and C. J. Pickard, Phys. Rev. B **84**, 174110 (2011).
[17] Z. G. Bazhanova, A. R. Oganov, and O. Gianola, Phys.-Usp. **55**, 489 (2012).
[18] J. Rouquette, D. Dolejš, I. Y. Kantor, C. A. McCammon, D. J. Frost, V. B. Prakapenka, and L. S. Dubrovinsky, Appl. Phys. Lett. **92**, 121912 (2008).
[19] L. Huang, N. V. Skorodumova, A. B. Belonoshko, B. Johansson, and R. Ahuja, Geophys. Res. Lett. **32**, L21314 (2005).

[20] C. Prescher, L. Dubrovinsky, E. Bykova, I. Kupenko, K. Glazyrin, A. Kantor, C. McCammon, M. Mookherjee, N. Nakajima, N. Miyajima, R. Sinmyo, V. Cerantola, N. Dubrovinskaia, V. Prakapenka, R. Rüffer, A. Chumakov, and M. Hanfland, Nat. Geosci. **8**, 220 (2015).
[21] G. Kresse and J. Furthmüller, Phys. Rev. B **54**, 11169 (1996).
[22] J. P. Perdew, K. Burke, and M. Ernzerhof, Phys. Rev. Lett. **77**, 3865 (1996).
[23] P. E. Blöchl, Phys. Rev. B **50**, 17953 (1994).
[24] G. Kresse and D. Joubert, Phys. Rev. B **59**, 1758 (1999).
[25] H. J. Monkhorst and J. D. Pack, Phys. Rev. B **13**, 5188 (1976).
[26] A. Togo, F. Oba, and I. Tanaka, Phys. Rev. B **78**, 134106 (2008).
[27] C. Prescher, L. Dubrovinsky, C. McCammon, K. Glazyrin, Y. Nakajima, A. Kantor, M. Merlini, and M. Hanfland, Phys. Rev. B **85**, 140402(R) (2012).
[28] A. V. Ruban and I. A. Abrikosov, Rep. Prog. Phys. **71**, 046501 (2008).
[29] M. Ekholm and I. A. Abrikosov, Phys. Rev. B **84**, 104423 (2011).
[30] Y. Fei and E. Brosh, Earth Planet. Sci. Lett. **408**, 155 (2014).
[31] L. V. Pourovskii, T. Miyake, S. I. Simak, A. V. Ruban, L. Dubrovinsky, and I. A. Abrikosov, Phys. Rev. B **87**, 115130 (2013).
[32] R. Dasgupta and D. Walker, Geochim. Cosmochim. Ac. **72**, 4627 (2008).